MicroRNA-199a-3p suppresses non-small cell lung cancer progression by targeting FTO to enhance m^{6}A-mediated downregulation of MZF1 and its transcriptional activation of CLDND1

YUZHEN CUI[1], XIAOQIAN LI[2], HONGKUI ZHANG[1], WEIQIANG YUAN[1] and ENBO ZHU[3]

[1]Department of Oncology, Yanbian University Affiliated Hospital, Yanji, Jilin 133000, P.R. China;
[2]Department of Nephrology, Yanbian University Affiliated Hospital, Yanji, Jilin 133000, P.R. China;
[3]Department of Neurology, Yanbian University Affiliated Hospital, Yanji, Jilin 133000, P.R. China

Received May 23, 2025; Accepted September 18, 2025

DOI: 10.3892/mmr.2025.13736

Abstract. The present study aimed to investigate the effect of microRNA (miR)-199a-3p on the biological function of non-small cell lung cancer (NSCLC) adenocarcinoma cells by targeting the fat mass and obesity-associated protein (FTO)/myeloid zinc finger 1 (MZF1)/claudin domain-containing 1 (CLDND1) axis. Human NSCLC cell lines, primarily A549 cells, were used for *in vitro* assays. Reverse transcription-quantitative PCR and western blotting were performed to assess the expression of relevant genes and proteins. Dual-luciferase reporter assays were used to verify the relationship between miR-199a-3p and FTO, as well as the transcriptional regulation of CLDND1 by MZF1. Methylated RNA immunoprecipitation was used to evaluate the N^6-methyladenosine (m^{6}A) modification levels of MZF1, whereas photoactivatable ribonucleoside-enhanced crosslinking and immunoprecipitation supported the binding of FTO to MZF1 mRNA. Cell proliferation, migration, invasion and apoptosis were assessed using Cell Counting Kit-8, Transwell and flow cytometry assays. miR-199a-3p was downregulated in NSCLC tissues and cells. Overexpression of miR-199a-3p inhibited A549 cell proliferation, invasion and migration. Mechanistically, miR-199a-3p directly targeted and suppressed FTO, an m^{6}A demethylase, leading to enhanced m6A modification of MZF1 mRNA and a subsequent decrease in MZF1 expression. Knockdown of MZF1 attenuated the oncogenic effects mediated by FTO, confirming that MZF1 served as a downstream effector of the miR-199a-3p/FTO axis. Moreover, MZF1 transcriptionally activated CLDND1, thereby facilitating the malignant phenotype of NSCLC cells. Collectively, these findings demonstrate that miR-199a-3p suppresses NSCLC progression by targeting FTO, promoting m^{6}A methylation-dependent downregulation of MZF1, and consequently decreasing CLDND1 expression. Thus, the miR-199a-3p/FTO/MZF1/CLDND1 axis may serve as a promising therapeutic target in NSCLC.

Correspondence to: Dr Enbo Zhu, Department of Neurology, Yanbian University Affiliated Hospital, 1327 Juzi, Yanji, Jilin 133000, P.R. China
E-mail: zhuenbo6071@163.com

Key words: non-small cell lung cancer, adenocarcinoma, microRNA-199a-3p, fat mass and obesity-associated protein, myeloid zinc finger 1, claudin domain containing 1, N^6-methyladenosine modification, proliferation, migration, invasion, apoptosis

Introduction

Lung cancer is a prevalent cause of cancer-related mortality and poses a notable health risk (1). Lung cancer comprises several histological subtypes, including adenocarcinoma, squamous carcinoma and large cell carcinoma, which are collectively known as non-small cell lung cancer (NSCLC) and small cell lung cancer (2). NSCLC accounts for 80-90% of all lung cancer cases (3). Because of the poor prognosis of NSCLC and limited treatment options due to issues such as late-stage drug resistance, there is a need to identify novel therapeutic targets and strategies (3,4). For diseases such as lung cancer, optimization of treatment strategies often requires multifaceted considerations.

The regulation of biological functions in lung cancer cells involves multiple levels and molecules. A preclinical study revealed the promise of microRNA (miRNA/miR) mimics and modulators in lung cancer therapy, potentially enhancing conventional treatments by reversing drug resistance and increasing cancer cell sensitivity (1). miRNA therapy has entered the clinical trial phase, demonstrating its safety and potential for therapeutic applications. For instance, the miRNA-16 mimic exhibited preliminary efficacy and tolerability in phase I clinical trials for NSCLC and malignant mesothelioma (5). The positive outcomes of the aforementioned preliminary trial provide evidence for miRNA replacement therapy. miR-199a exhibits tumor-suppressive effects in NSCLC by inhibiting growth and metastasis *in vivo* (6). miR-199a can inhibit the

development of lung cancer, particularly by suppressing the proliferation, migration and infiltration of lung cancer cells, as well as by inhibiting tumor angiogenesis and promoting lung cancer cell apoptosis, thereby influencing lung cancer cell drug resistance (7). miR-199a comprises two mature forms, miR-199a-3p and miR-199a-5p, both of which serve important biological roles (7). A previous study has revealed that miR-199a-3p/5p was downregulated in NSCLC tissues, cell lines and patient samples, and its overexpression inhibited the malignant behavior of cells (6). Overexpression of miR-199a-3p markedly inhibits cell proliferation, migration and invasion in esophageal squamous cell carcinoma (8). Additionally, miR-199a-3p is substantially downregulated in nasopharyngeal carcinoma tissues and cells, and it can inhibit the migration and invasion of nasopharyngeal carcinoma cells by downregulating stearoyl-CoA desaturase 1 expression (9). However, the specific mechanism of action of miR-199a-3p in NSCLC remains to be elucidated. Therefore, the present study focused on miR-199a-3p and explored its potential as a therapeutic target.

Fat mass and obesity-associated protein (FTO) was the first identified RNA N^6-methyladenosine (m^6A) demethylase in eukaryotic cells, and regulates m^6A levels in mRNAs and serves a key role in tumor progression and drug resistance, including in lung cancer (10,11). m^6A is the most abundant internal mRNA modification that regulates processes such as alternative splicing and translation (11). Transcriptome-wide m^6A maps, known as the epitranscriptome, reveal the distribution and patterns of m^6A in cellular RNAs. These maps reveal specific mRNAs regulated by m^6A, providing mechanistic links between m^6A and cell differentiation, cancer progression and other processes (12). FTO promotes adipogenesis by regulating the adipogenic pathway (13). m^6A and FTO levels are dysregulated in multiple cancer types, including lung cancer (11). A study by Xu *et al* (14) reported that FTO expression was lower in NSCLC samples compared with healthy tissues and was negatively associated with poor prognosis. Functional assays have revealed that FTO inhibits NSCLC tumor cell proliferation and metastasis *in vitro* and *in vivo* (14). However, a previous study has reported an oncogenic role of FTO in acute myeloid leukemia (15). This discrepancy suggests that FTO functions are tissue- or cell-context-dependent.

Myeloid zinc finger 1 (MZF1), a SCAN-domain zinc finger transcription factor associated with numerous types of cancers, shows decreased expression in pancreatic cancer and NSCLC tumors compared to normal tissues (16). High MZF1 expression is associated with lower overall survival in patients with glioblastoma multiforme (17). However, the specific role of MZF1 in lung cancer remains to be fully elucidated.

Claudin domain-containing 1 (CLDND1), also known as claudin-25, has been identified as a novel member of the claudin protein family (18). Claudins serve important roles in intercellular adhesion. Elevated expression of CLDND1 is associated with malignant progression in estrogen receptor-negative, hormone therapy-resistant breast cancer. Aberrant CLDND1 levels are also linked to vascular pathologies (19). A study investigating the regulation of CLDND1 expression identified a strong enhancer region near its promoter that shares high homology with the ETS domain-containing protein Elk-1 (ELK1) binding sequence, suggesting that CLDND1 may be a potential target for anticancer drug development (19). However, to the best of our knowledge, no studies have investigated the specific role of CLDND1 in the development of lung cancer.

The present study aimed to investigate a novel signaling axis involving miR-199a-3p, FTO, MZF1, and CLDND1 in NSCLC. Bioinformatics tools including miRwalk were employed to predict potential downstream targets of miR-199a-3p. The SRAMP online tool was utilized to assess the potential for m^6A modification in MZF1 mRNA, while the JASPAR database was used to analyze the binding affinity of MZF1 to the CLDND1 promoter region. It was hypothesized that FTO, as an m^6A demethylase, may regulate MZF1 expression via m^6A modification, thereby influencing CLDND1 transcription and contributing to NSCLC progression. The study was designed to experimentally validate this proposed miR-199a-3p/FTO/m^6A/MZF1/CLDND1 axis, with the goal of elucidating its functional role in NSCLC and exploring its potential as a diagnostic or therapeutic target.

Materials and methods

Ethics statement. The present study was approved by the Ethics Committee of Yanbian University Affiliated Hospital (approval no. 2021094; Yanji, China), and written informed consent was obtained from all patients. The study adhered to the principles outlined in The Declaration of Helsinki.

Clinical samples. Lung cancer tissue specimens were collected from 15 patients with NSCLC (adenocarcinoma) who underwent surgical resection at Yanbian University Affiliated Hospital (Yanji, China) between January 2022 and June 2023. For each patient, a paired paracancerous tissue specimen (≥5 cm from the tumor margin and pathologically confirmed to be free of tumor cell infiltration) was simultaneously collected.

Inclusion criteria were: i) histopathological confirmation of primary NSCLC (adenocarcinoma), ii) no prior neoadjuvant chemotherapy, radiotherapy, or targeted therapy before surgery, and iii) availability of complete clinicopathological data. Exclusion criteria were: i) presence of other malignant tumors or severe systemic diseases, ii) history of autoimmune or infectious diseases, and iii) inadequate tissue quantity or RNA quality. Immediately after resection, all tissue specimens were snap-frozen in liquid nitrogen and stored at -80˚C until further analysis to preserve molecular integrity.

A priori power analysis was performed using G*Power 3.1 (Heinrich Heine University Düsseldorf, Germany), setting α=0.05 and an effect size=0.8, which indicated that n=15 achieves a statistical power >85%. Patients' ages ranged from 35 to 69 years (median=52 years). All diagnoses were confirmed by the Department of Pathology. The clinical characteristics of patients with NSCLC are shown in Table SI.

Cell culture and grouping. CAL12T (cat. no. MZ-8194), HCC44 (cat. no. MZ-8190), NCIH1993 (cat. no. MZ-8234) and A549 (cat. no. B163886) lung cancer cells, and BEAS-2B human normal bronchial epithelial cells (cat. no. MZ-0677), were obtained from Ningbo Mingzhou Biotechnology Co., Ltd. All cells were cultured in DMEM; cat. no. 11965092; Gibco, Thermo Fisher Scientific, Inc.) supplemented with 10% fetal

bovine serum (FBS; cat. no. 10099141C; Gibco, Thermo Fisher Scientific, Inc.) and 1% penicillin-streptomycin (100 U/ml penicillin, 100 μg/ml streptomycin; cat. no. 15140122; all Gibco) at 37˚C in a humidified incubator containing 5% CO_2. Cells were sub-cultured at 70-80% confluence using 0.25% trypsin-EDTA (HyClone; Cytiva), and only cells in the logarithmic growth phase were used for experiments. All cell lines were authenticated via short tandem repeat analysis and regularly tested for the absence of mycoplasma contamination (Table SII).

The A549 cells were divided into the following groups based on the experimental needs: i) miR-199a-3p mimic group transfected with miR-199a-3p mimic; ii) negative control (NC) mimic group transfected with miR-199a-3p mimic NC sequence; iii) NC mimic + overexpression (oe)-NC group transfected with miR-199a-3p mimic NC sequence and FTO overexpression NC plasmid; iv) miR-199a-3p mimic + oe-NC group transfected with miR-199a-3p mimic and FTO overexpression NC plasmid; v) NC mimic + oe-FTO group transfected with miR-199a-3p mimic NC sequence and FTO overexpression plasmid; vi) miR-199a-3p mimic + oe-FTO group transfected with miR-199a-3p mimic and FTO overexpression plasmid; vii) oe-NC group transfected with overexpression NC plasmid; viii) oe-FTO group transfected with FTO overexpression plasmid; ix) oe-MZF1 group transfected with MZF1 overexpression plasmid; x) oe-NC + short hairpin RNA (sh)-NC group transfected with FTO overexpression and MZF1 silencing NC plasmid; xi) oe-FTO + sh-NC group transfected with FTO overexpression plasmid and MZF1 silencing NC plasmid; xii) oe-NC + sh-MZF1 group transfected with FTO overexpression NC plasmid and MZF1 silencing plasmid; xiii) oe-FTO + sh-MZF1 group transfected with FTO overexpression plasmid and MZF1 silencing plasmid; xiv) oe-MZF1 + sh-NC group transfected with MZF1 overexpression plasmid and CLDND1 silencing NC plasmid; xv) oe-NC + sh-CLDND1 group transfected with MZF1 overexpression and CLDND1 silencing plasmid; and xvi) oe-MZF1 + sh-CLDND1 group transfected with MZF1 overexpression plasmid and CLDND1 silencing plasmid.

The FTO and MZF1 oe plasmids were constructed using the pCMV6-AC-GFP vector (Hunan Fenghui Biotechnology Co., Ltd.; cat. no. ZT877), and the MZF1 and CLDND1 silencing plasmids (sh-MZF1, sh-CLDND1) along with their negative controls (sh-NC) were generated using the pGPU6-GFP-Neo backbone (Hunan Fenghui Biotechnology Co., Ltd.; cat. no. BR150). Synthetic miR-199a-3p mimic and NC mimic were purchased from Shanghai GenePharma Co., Ltd., and prepared at a working concentration of 50 nM. All nucleic acids were transfected using Lipofectamine® 2000 (cat. no. 11668019; Invitrogen, Thermo Fisher Scientific, Inc.) following the manufacturer's protocol. For each well of a 6-well plate, 4 μg plasmid DNA or 50 nM miRNA mimic was mixed with 10 μl Lipofectamine 2000 in 250 μl serum-free Opti-MEM (Gibco; Thermo Fisher Scientific, Inc.) at 37˚C with 5% CO_2 for 6 h before the medium was replaced with complete DMEM, and harvested 24-48 h post-transfection for subsequent assays (Fig. S1) (20). Sequence information is shown in Table SIII.

Reverse transcription-quantitative PCR (RT-qPCR). Total RNA was extracted from A549 cells and human NSCLC tumor and paired paracancerous tissue using TRIzol (Invitrogen; Thermo Fisher Scientific, Inc.) following the manufacturer's instructions. cDNA was synthesized with the PrimeScript RT reagent kit with gDNA Eraser (cat. no. RR047A; Takara Bio, Inc.) using the following program: genomic DNA removal at 42˚C for 2 min, reverse transcription at 37˚C for 15 min, and enzyme inactivation at 85˚C for 5 sec. For miRNA analysis, cDNA was generated using the miRNA First Strand cDNA Synthesis (Tailing Reaction) kit (cat. no. B532451-0020; Sangon Biotech Co., Ltd.) with a tailing/RT program of 37˚C for 60 min followed by 85˚C for 5 min. qPCR was performed on a 7900HT Fast Real-Time PCR System (Applied Biosystems, Thermo Fisher Scientific, Inc.) using SYBR™ Green PCR Master Mix (Applied Biosystems). The thermal cycling conditions were: 95˚C for 10 min, then 40 cycles of 95˚C for 15 sec and 60˚C for 60 sec; melt-curve analysis was conducted from 60-95˚C with a gradual ramp. The relative gene expression levels were calculated using the $2^{-\Delta\Delta Cq}$ method (21), with U6 as the internal reference for miRNA and GAPDH as the reference for mRNA. All primers were purchased from Sangon Biotech Co., Ltd. (Table I) (22). The experiment was repeated three times.

Western blot analysis. Total protein was extracted from human NSCLC tumor and paired paracancerous tissue using RIPA lysis buffer (cat. no. P0013C; Beyotime Institute of Biotechnology) containing 1 mM phenylmethylsulfonyl fluoride. Following centrifugation at 12,000 x g for 10 min at 4˚C, the supernatant was collected, and the protein concentration was quantified using a BCA Protein Assay Kit (cat. no. 23227; Thermo Fisher Scientific, Inc.). Equal amounts of protein (30 μg per lane) were loaded and separated by 10% SDS-polyacrylamide gel electrophoresis (PAGE), followed by transfer onto polyvinylidene difluoride (PVDF) membranes. The membranes were blocked with 5% non-fat dry milk (BD Difco™; BD Biosciences) in Tris-buffered saline with 0.1% Tween-20 (TBST) at room temperature for 1 h, then incubated overnight at 4˚C with primary antibodies as follows: Rabbit anti-FTO (1:1,000; cat. no. ab126605; Abcam), anti-MZF1 (1:800; cat. no. ab64866; Abcam) and anti-CLDND1 (1:1,000; cat. no. 13255; Cell Signaling Technology, Inc.). Anti-GAPDH (1:2,500; cat. no. ab9485; Abcam) was used as an internal reference. After washing with TBST, membranes were incubated with HRP)-conjugated goat anti-rabbit IgG H&L (1:2,000; cat. no. ab97051; Abcam) for 1 h at room temperature. Equal volumes of liquids A and B from an ECL fluorescence testing kit [cat. no. abs920; Absin Bioscience Inc.] were mixed in a dark room and added dropwise to the membrane. Protein signals were captured using the Bio-Rad Image Analysis System (Bio-Rad Laboratories, Inc.) with an exposure time ranging between 10 and 30 sec, dynamically adjusted based on signal intensity to ensure optimal image quality without saturation. Image grayscale values were analyzed using Quantity One v4.6.2 software (Bio-Rad Laboratories, Inc.), and relative protein content was expressed as the grayscale value of the corresponding protein band divided by the grayscale value of the GAPDH protein band. The relative protein content was calculated based on the gray value ratio of the target protein to GAPDH (23).

Table I. Primer sequences for reverse transcription-quantitative PCR.

Gene	Primer sequence, 5'→3'
miR-199a-3p (human)	
Forward	ACAGTAGTCTGCACATTGGTTA
Reverse	GTGCAGGGTCCGAGGT
FTO (human)	
Forward	GTTCACAACCTCGGTTTAGTTC
Reverse	CATCATCATTGTCCACATCGTC
MZF1 (human)	
Forward	TTCCGGTGCTTCCGCTATG
Reverse	CTCCTTGGAGCGTACCTCT
CLDND1 (human)	
Forward	TGGTATAGCCCACCAGAAAGGAC
Reverse	CAATCCCGCTATTGTGGTTTCCG
U6 (human)	
Forward	CTCGCTTCGGCAGCACA
Reverse	AACGCTTCACGAATTTGCGT
GAPDH (human)	
Forward	GGAGCGAGATCCCTCCAAAAT
Reverse	GGCTGTTGTCATACTTCTCATGG

miR, microRNA; FTO, fat mass and obesity-associated protein; MZF1, myeloid zinc finger 1; CLDND1, claudin domain-containing 1.

Dual-luciferase reporter assay. The miRwalk biological website (http://mirwalk.umm.uni-heidelberg.de/) was utilized for analysis and predicted that the miR-199a-3p sequence contained binding sites for FTO. To verify this interaction, wild-type (Wt) and mutant (Mut) 3'-UTR fragments of FTO were synthesized and cloned into the pGL3-Control vector (cat. no. E1741; Promega Corporation) to generate pGL3-FTO-Wt and pGL3-FTO-Mut constructs. The Mut plasmid was obtained by site-directed mutagenesis within the miR-199a-3p seed region (for example, A replaced with T). Synthetic miR-199a-3p mimic (5'-ACAGUAGUCUGCACAUUGGUU A-3') and negative control mimic (miR-NC) (5'-UUCUCC GAACGUGUCACGUTT-3') were purchased from Shanghai GenePharma Co., Ltd. For luciferase reporter analysis, A549 cells were co-transfected with 100 ng of PGLO-FTO-Wt or PGLO-FTO-Mut vector and 50 nM miR-199a-3p mimic or miR-NC using Lipofectamine® 2000 (cat. no. 11668019; Invitrogen; Thermo Fisher Scientific, Inc.), the same reagent and protocol described above (24).

The binding site of the transcription factor MZF1 was obtained from the JASPAR website (jaspar.genereg.net/). To evaluate the regulatory effect of MZF1 on the CLDND1 promoter, oe-NC and oe-MZF1 plasmids were co-transfected with reporter constructs containing either the Wt or Mut CLDND1 promoter sequences cloned upstream of the luciferase gene in the pGL3-Basic vector (cat. no. E1751; Promega), which lacks a promoter and is suitable for promoter-driven transcriptional analysis. A pRL-TK Renilla luciferase plasmid (cat. no. E2241; Promega) was co-transfected as an internal control. Cells were collected and lysed 48 h post-transfection, and dual-luciferase activity was quantified using the same assay kit.

Firefly luciferase activity was first determined by adding 100 μl Luciferase Assay Reagent II to each lysate, followed by Renilla luciferase measurement with 100 μl Stop & Glo® Reagent using a GloMax® 20/20 Luminometer (Promega). The relative luciferase activity was calculated as the ratio of firefly to Renilla luminescence, expressed as relative light units (RLU). Each experiment was independently repeated three times to ensure reproducibility (25).

Chromatin immunoprecipitation (ChIP). A ChIP kit (cat. no. KT101; Guangzhou Saicheng Biotechnology Co., Ltd.) was used to detect the enrichment of MZF1 in the promoter region of the CLDND1 gene. When A549 cells reached 70-80% confluence, they were crosslinked with 1% formaldehyde for 10 min at room temperature, and the reaction was quenched with 125 mM glycine for 5 min. Cells were collected by centrifugation at 12,000 x g for 10 min at 4˚C, washed twice with cold PBS, and lysed in SDS lysis buffer (1% SDS, 10 mM EDTA, 50 mM Tris-HCl, pH 8.1) containing protease inhibitor cocktail. After incubation on ice for 10 min, the lysates were subjected to sonication at 20 kHz with 30/30 sec off cycles for a total of 10 min at 4˚C to shear chromatin and obtain DNA fragments of 200-500 bp. For each immunoprecipitation, chromatin from ~1x10^6 cells (≈500 μl total volume) was diluted in ChIP dilution buffer and incubated overnight at 4˚C with either 2 μg rabbit anti-MZF1 antibody (cat. no. ab64866, Abcam, UK) or 2 μg normal rabbit IgG (cat. no. ab172730, Abcam) as a NC. The immune complexes were captured with 25 μl Protein G magnetic beads for 2 h at 4˚C with rotation. Beads were separated on a magnetic rack, and washed three times with low-salt buffer (20 mM Tris-HCl, pH 8.1; 150 mM NaCl; 2 mM EDTA; 1% Triton X-100; 0.1% SDS), high-salt buffer (same as above except 500 mM NaCl), LiCl buffer (10 mM Tris-HCl, pH 8.1; 250 mM LiCl; 1% NP-40; 1% sodium deoxycholate; 1 mM EDTA) and TE buffer (10 mM Tris-HCl, pH 8.0; 1 mM EDTA). Chromatin complexes were eluted twice with 1% SDS/0.1 M $NaHCO_3$ elution buffer at 65˚C for 15 min, pooled, and reverse-crosslinked overnight at 65˚C. Samples were treated sequentially with RNase A (37˚C, 30 min) and Proteinase K (55˚C, 1 h), and DNA was purified using silica-membrane spin columns (Qiagen DNA Cleanup Kit). Purified DNA was subjected to qPCR to detect MZF1 binding to the CLDND1 promoter as aforementioned. This amplified fragment spans nucleotides -1017 to +192 relative to the transcription start site of the CLDND1 promoter (GenBank Accession No. NM_001040181) (26). The experiment was repeated three times.

Methylated RNA immunoprecipitation (Me-RIP). The SRAMP online tool (cuilab.cn/sramp; version 2023-10) was used to predict potential m^6A modification sites in MZF1 mRNA. Total RNA was isolated from A549 cells using the TRIzol method as previously described (27), and mRNA was isolated and purified using the PolyATtract mRNA Isolation System [cat. no. A-Z5300; Aide Technology (Beijing) Co., Ltd.]. An aliquot of 5 μg purified mRNA was diluted in

500 μl MeRIP lysis buffer (150 mM NaCl, 10 mM Tris-HCl pH 7.4, 0.1% NP-40, 1 mM EDTA, 1x RNase inhibitor, and 1x protease inhibitor cocktail) and incubated with 30 μl Protein A/G magnetic beads (Thermo Fisher Scientific) pre-bound to antibodies for immunoprecipitation. Anti-m^{6}A antibody (2 μg;1:500; cat. no. ab151230; Abcam) or anti-IgG antibody (2 μg;1:100; cat. no. ab109489; Abcam) was incubated with Protein A/G beads in binding buffer at 4˚C for 1 h with gentle rotation to form antibody-bead complexes. The prepared RNA-antibody-bead mixture was incubated overnight at 4˚C. The beads were magnetically separated and washed three times with low-salt buffer (50 mM Tris-HCl, pH 7.4; 150 mM NaCl; 0.1% NP-40; 0.5 mM EDTA) and once with high-salt buffer (same composition but 500 mM NaCl) to remove non-specific binding. Each wash was performed for 5 min at 4˚C with rotation. Beads were suspended in 100 μl elution buffer (6.7 mM m^{6}A-free N^6-methyladenosine solution, 50 mM Tris-HCl, pH 7.4, 10 mM EDTA) and incubated at 55˚C for 1 h to release methylated RNA. The eluate was subjected to phenol-chloroform extraction and RNA was precipitated with ethanol, followed by resuspension in RNase-free water. RNA concentration and purity were measured with a NanoDrop 2000 spectrophotometer (Thermo Fisher Scientific). RNA was eluted with elution buffer, purified by phenol-chloroform extraction and analyzed by RT-qPCR for MZF1 as aforementioned. Primer sequences targeting the conserved exonic regions of MZF1 were designed using Primer-BLAST (National Center for Biotechnology Information, database version 2024-03) and are listed in Table I (28,29).

Photoactivatable ribonucleoside-enhanced crosslinking and immunoprecipitation (PAR-CLIP). A549 cells were incubated with 200 μM 4-thiouridine for 16 h, then UV-irradiated at 365 nm (0.4 J/cm^2) on ice. Cells were lysed in PAR-CLIP buffer (20 mM Tris-HCl, pH 7.5, 150 mM NaCl, 1 mM $MgCl_2$, 0.5% NP-40, 1 mM DTT, RNase and protease inhibitors) and cleared by centrifugation (12,000 x g, 10 min, 4˚C). Supernatant (500 μl) were incubated overnight at 4˚C with 2 μg anti-FTO antibody (ab126605, Abcam, UK) or 2 μg rabbit IgG (cat. no. ab172730, Abcam) and 30 μl Protein A/G magnetic beads (Thermo Fisher Scientific). Beads were magnetically separated, washed three times with high-salt buffer (50 mM Tris-HCl pH 7.4, 500 mM NaCl, 1 mM EDTA, 0.1% NP-40) and once with low-salt buffer (150 mM NaCl). The precipitated RNA was labeled with (γ-32P)-ATP using T4 polynucleotide kinase (New England Biolabs) for 30 min at 37˚C, resolved by 10% SDS-PAGE, transferred to nitrocellulose, and visualized by autoradiography. Crosslinked RNA was recovered after Proteinase K digestion (0.5 mg/ml, 37˚C, 30 min) and phenol-chloroform extraction. Recovered RNA was reverse-transcribed with the PrimeScript™ RT Reagent Kit (RR047A; Takara Bio, Japan) and analyzed by RT-qPCR as aforementioned (30). The experiment was repeated three times.

Transwell assay. Cell migration and invasion were assessed using Transwell 24-well cell culture inserts (6.5 mm diameter, 8.0 μm pore; cat. no. 3422; Corning, Inc.). For the invasion assay, Matrigel® gel (cat. no. 356234; Corning, Inc.) was added at 37˚C for 30-60 min. A549 cells in the logarithmic phase were trypsinized, counted, and resuspended in serum-free DMEM. For each insert, 200 μl of cell suspension containing 1x10^5 cells was added to the upper chamber. The lower chamber was filled with 800 μl DMEM supplemented with 20% FBS to serve as a chemoattractant. All plates were incubated at 37˚C in a 5% CO_2 atmosphere for 24 h. For the migration assay, the procedure was identical except that the inserts were not pre-coated with Matrigel. After incubation, non-migrated or non-invaded cells on the upper surface were gently removed with a cotton swab. The membranes were fixed with 4% paraformaldehyde for 15 min at room temperature, stained with 0.1% crystal violet solution (cat. no. C0121; Beyotime Biotechnology) at room temperature for 20 min, and washed twice with PBS. Cells that migrated or invaded the lower surface of the membrane were visualized and counted under an inverted light microscope (Eclipse TE2000; Nikon Corporation, Tokyo, Japan). To ensure accuracy, cells from at least four randomly selected microscopic areas were counted (31).

Cell Counting Kit-8 (CCK-8) assay. Cell proliferation was evaluated using CCK-8 (cat. no. CA1210; Beijing Solarbio Science & Technology Co., Ltd.). A549 cells in the logarithmic growth phase were seeded into 96-well plates at a density of 1x10^4 cells/well in 100 μl complete medium and cultured for 24 h to allow cell adherence and recovery prior to transfection. Cells were then transfected according to the experimental grouping, and proliferation was assessed beginning 48 h after transfection. At 0, 24, 48, and 72 h after the onset of proliferation monitoring (i.e., after transfection), 10 μl CCK-8 reagent was added to each well, followed by incubation at 37˚C for 3 h. The absorbance at 450 nm was measured using a microplate reader (Multiskan™ FC, Thermo Fisher Scientific, USA). The absorbance was directly proportional to the number of proliferating cells in the culture medium, and a cell growth curve was plotted based on these values (32). The experiment was repeated three times.

Flow cytometry. After 48 h of transfection, the A549 cells were digested with 0.25% trypsin (cat. no. 15050057; Gibco; Thermo Fisher Scientific Inc.) and collected in a flow-through tube. Cell suspensions were centrifuged at 300 x g for 5 min at 4˚C, and the supernatant was discarded. An Annexin-V-FITC apoptosis detection kit (cat. no. ab14085; Abcam) was used to formulate the Annexin V-FITC/PI staining solution at a ratio of 1:2:50 by mixing Annexin-V-FITC, PI and HEPES buffer solutions according to the manufacturer's instructions. A total of 1x10^6 cells were resuspended per 100 μl of the staining solution, and after 15 min of incubation at room temperature, 1 ml HEPES buffer solution (cat. no. PB180325; Procell Life Science & Technology Co., Ltd.) was added. Fluorescence was detected using a BD FACSCanto™ II flow cytometer (BD Biosciences), with FITC and PI emissions collected at 525 nm and 620 nm, respectively, after excitation at 488 nm. Data were analyzed using FlowJo software (version 10.8.1; BD Biosciences). Results were expressed as the percentage of apoptotic cells (Annexin V$^+$/PI$^+$ and Annexin V$^+$/PI$^-$ fractions) to ensure quantitative reproducibility (33). The experiment was repeated three times.

Statistical analysis. All experiments were conducted with at least three independent replicates (n=3), and data are presented as the mean ± SD. For comparisons between two independent (unpaired) groups, an unpaired two-tailed Student's t-test was used. For paired designs, a paired two-tailed Student's t-test was applied. By contrast, for three or more treatment groups, one-way ANOVA was employed, supplemented with Tukey's post hoc multiple comparison test, for comparisons involving multiple time points. For comparisons involving both time and treatment factors, two-way ANOVA was used. The Sidak methods were selected for post hoc multiple comparisons at each time point. All statistical tests were two-sided, with $P<0.05$ considered to indicate a statistically significant difference, and actual P-values were retained to three decimal places. Error bars in the graphs indicate the-SD. All statistical analyses were performed using GraphPad Prism 6.0 (Dotmatics).

Results

miR-199a-3p expression is significantly downregulated in NSCLC tissues and cells. In the study of the molecular mechanisms of lung cancer, the expression patterns of miRNAs have received notable attention, and the aberrant expression of several miRNAs in lung cancer has been reported to be closely related to cancer progression (34). The RT-qPCR results in the present study showed that the expression levels of miR-199a-3p were significantly downregulated in NSCLC tissues compared with normal tissues (Fig. 1A). Furthermore, miR-199a-3p expression was also assessed in various lung cancer cell lines. The present results showed that in the lung cancer cell lines, the expression levels of miR-199a-3p were significantly downregulated, with the A549 cell line having the lowest expression level (Fig. 1B). Therefore, the A549 cell line was selected for subsequent in-depth study.

miR-199a-3p inhibits A549 cell proliferation, migration and invasion by targeting FTO inhibition. To elucidate the mechanism of action of miR-199a-3p in A549 cells, bioinformatics tools were used to predict the potential downstream target genes of miR-199a-3p, which led to the identification of FTO as a potential direct target (Fig. 2A). A previous study reported an oncogenic role of FTO in acute myeloid leukemia (15). To validate whether FTO exhibits similar dysregulation in NSCLC, FTO mRNA and protein expression levels were analyzed in paired NSCLC and adjacent normal tissue, as well as in lung cell lines. The results of RT-qPCR and western blotting revealed that both FTO mRNA and protein expression were significantly upregulated in NSCLC tissues compared with the adjacent normal tissues (Fig. 2B). Consistently, FTO mRNA expression was markedly higher in NSCLC cell lines (A549, CAL12T, HCC44, and NCI-H1993) than in the normal human bronchial epithelial cell line BEAS-2B (Fig. 2C).

In subsequent experiments, A549 cells were transfected with miR-199a-3p mimic and NC mimic, and the expression levels of miR-199a-3p and FTO in transfected cells were analyzed by RT-qPCR. The results showed that the expression levels of miR-199a-3p were significantly increased in the miR-199a-3p mimic group compared with the NC mimic group. At the same time, FTO expression was significantly decreased in the miR-199a-3p mimic group compared with the NC mimic group, suggesting miR-199a-3p negatively regulated FTO expression (Fig. 2D).

Dual-luciferase reporter assays were conducted to verify the direct targeting relationship between miR-199a-3p and FTO. The Wt and Mut sequences of the FTO 3'-UTR were co-transfected with miR-199a-3p mimic into A549 cells. The results revealed that in the cells co-transfected with the FTO-Wt 3'-UTR, the luciferase activity was significantly lower in the miR-199a-3p mimic group compared with the NC mimic group. However, in the cells co-transfected with the FTO-Mut 3'-UTR, there was no significant difference in luciferase activity between the two mimic groups, indicating that miR-199a-3p specifically targeted the FTO 3'-UTR (Fig. 2E).

RT-qPCR results revealed that, compared with those in the NC mimic + oe-NC group, the expression levels of FTO were significantly reduced in cells in the miR-199a-3p mimic + oe-NC group. When FTO was overexpressed, its expression level in the miR-199a-3p mimic + oe-FTO group was significantly higher than that in the miR-199a-3p mimic + oe-NC group (Fig. 2F). Cell proliferation, migration, and invasion were significantly reduced, whereas apoptosis was markedly increased, in the miR-199a-3p mimic + oe-NC group compared with the NC mimic + oe-NC group. By contrast, cells transfected with NC mimic + oe-FTO exhibited increased proliferation, migration, and invasion and decreased apoptosis relative to the corresponding controls, indicating a tumor-promoting effect of FTO overexpression. Furthermore, co-transfection of miR-199a-3p mimic with oe-FTO partially restored the proliferative, migratory, and invasive capacities that had been suppressed by miR-199a-3p alone (Fig. 2G-I).

In summary, the present study demonstrated that miR-199a-3p inhibited the proliferation, migration and invasion of A549 cells by targeting FTO. This revealed the important role of the miR-199a-3p/FTO axis in regulating the behavior of A549 cells and provided potential novel targets for molecularly targeted therapy of NSCLC.

m^6A demethylase FTO promotes MZF1 expression by reducing the levels of m^6A modification of MZF1. A previous study reported that MZF1 promotes tumorigenesis and metastasis (35), and an online website analysis showed that MZF1 mRNA can undergo m^6A modification (Fig. 3A). Therefore, we hypothesized that FTO, an m^6A demethylase, affects tumor progression by regulating the m^6A modification of MZF1.

Expression levels of MZF1 were examined in NSCLC tissues and cell lines by RT-qPCR and western blot analyses. As shown in Fig. 3B, both the mRNA and protein levels of MZF1 were significantly higher in NSCLC tumor tissues than in their paired adjacent normal tissues. Consistently, MZF1 mRNA expression was markedly upregulated in NSCLC cell lines (CAL12T, HCC44, A549, and NCI-H1993) compared with BEAS-2B, with the highest expression observed in A549 cells (Fig. 3C). Subsequently, FTO was overexpressed in the cells; overexpression of FTO significantly increased the mRNA expression levels of MZF1 (Fig. 3D).

To determine how FTO regulated MZF1, the m^6A modification level of MZF1 after FTO overexpression was examined using a Me-RIP assay. FTO overexpression significantly reduced the m^6A modification of MZF1 mRNA compared with

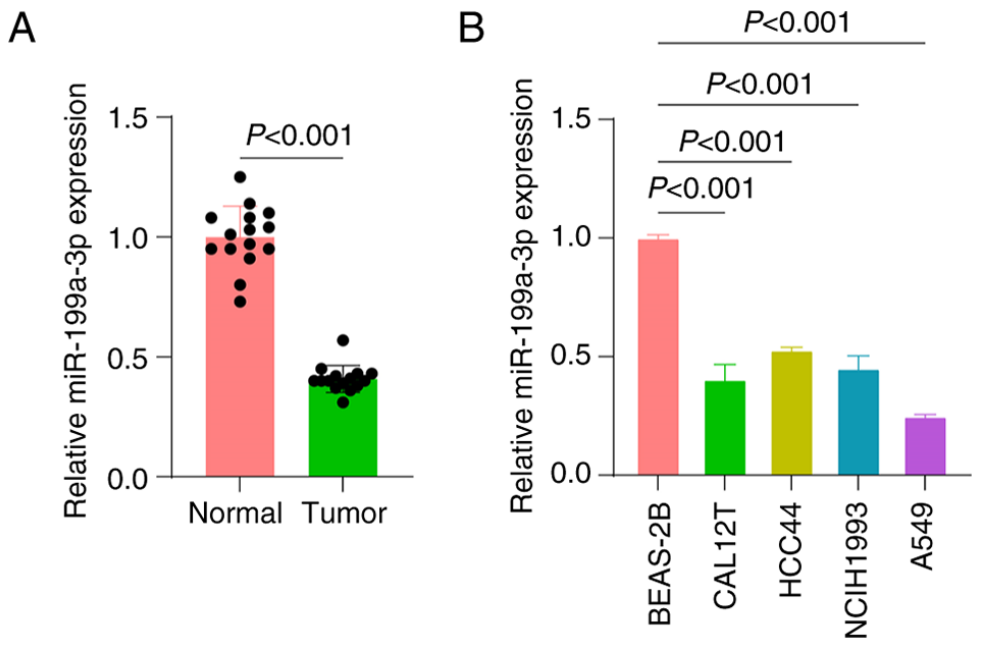

Figure 1. Expression levels of miR-199a-3p in NSCLC tissues and cells. (A) RT-qPCR was utilized to test the expression level of miR-199a-3p in NSCLC tissues, and paracancerous tissues were regarded as the control (n=15). (B) RT-qPCR was performed to detect miR-199a-3p expression in normal bronchial epithelial cells (BEAS-2B) and NSCLC cell lines (A549, H1299, H460 and H1975). Data are presented as the mean ± SD from three independent experiments (n=3). All cell experiments were repeated three times. RT-qPCR, reverse transcription-quantitative PCR; miR, microRNA; NSCLC, non-small cell lung cancer.

the oe-NC group (Fig. 3E). Additionally, a PAR-CLIP assay was employed to investigate the direct interaction between FTO and MZF1 mRNA. The anti-m^{6}A antibody pulled down significantly more MZF1 mRNA than the anti-IgG control, and the enrichment was markedly higher in the oe-FTO group than in the oe-NC group (Fig. 3F).

Taken together, the present data demonstrated that FTO could promote MZF1 expression by reducing the m^{6}A modification level of MZF1 mRNA.

Silencing of MZF1 reverses the promoting effect of FTO on A549 cell proliferation, migration and invasion. To further ascertain the effect of the FTO/MZF1 axis on the biological function of A549 cells, three groups were established: oe-NC + sh-NC, oe-FTO + sh-NC, and oe-FTO + sh-MZF1. RT-qPCR demonstrated that the expression levels of both FTO and MZF1 were significantly elevated in the cells in the oe-FTO + sh-NC group compared with the oe-NC + sh-NC group, and the expression levels of MZF1 were significantly lower in the cells in the oe-FTO + sh-MZF1 group compared with the oe-FTO + sh-NC group (Fig. 4A).

The biological functions of A549 cells were evaluated using CCK-8, Transwell and flow cytometry assay. The results revealed that, compared with the oe-NC + sh-NC group, the oe-FTO + sh-NC group exhibited significantly higher cell proliferation, migration and invasion, as well as a significantly lower apoptosis. When MZF1 was silenced, the effect of FTO was partially reversed, as demonstrated by the significant decrease in proliferation, migration and invasion in the oe-FTO + sh-MZF1 group compared with the oe-FTO + sh-NC group, as well as a significant increase in apoptosis (Fig. 4B-D).

Taken together, the present study demonstrated that silencing of MZF1 reversed the promoting effect of FTO on A549 cell proliferation, migration and invasion.

MZF1 promotes A549 cell proliferation, migration and invasion by facilitating CLDND1 transcription. MZF1 is a transcription factor that can influence tumor progression by promoting downstream gene expression (36). The binding site of the transcription factor MZF1 was obtained from the JASPAR website (https://jaspar.genereg.net/) (Fig. 5A), and MZF1 showed a high binding affinity (GAAATCCCCTATT) for the CLDND1 promoter region. CLDND1 expression was significantly higher in NSCLC tumor tissues than in adjacent normal tissue (Fig. 5B). Consistently, CLDND1 mRNA levels were markedly elevated in A549 and other NSCLC cell lines (NCI-H1993, CAL12T, HCC44) compared with BEAS-2B cells (Fig. 5C).

To explore the regulatory effect of MZF1 on CLDND1, MZF1 was overexpressed in A549 cells. RT-qPCR results revealed that MZF1 overexpression significantly elevated the mRNA levels of CLDND1 (Fig. 5D). In addition, a dual-luciferase reporter assay revealed that overexpression of MZF1 significantly increased the luciferase activity of the wild-type (CLDND1-Wt) promoter reporter compared with the oe-NC group, whereas no significant change was observed in the mutant (CLDND1-Mut) reporter lacking the predicted MZF1 binding motif (Fig. 5E).

ChIP experiments indicated that MZF1 directly regulated the CLDND1 promoter, showing a significant increase in MZF1 enrichment in the CLDND1 promoter region (Fig. 5F).

In the cell function experiments, the effects of different transfection combinations on the proliferation, migration

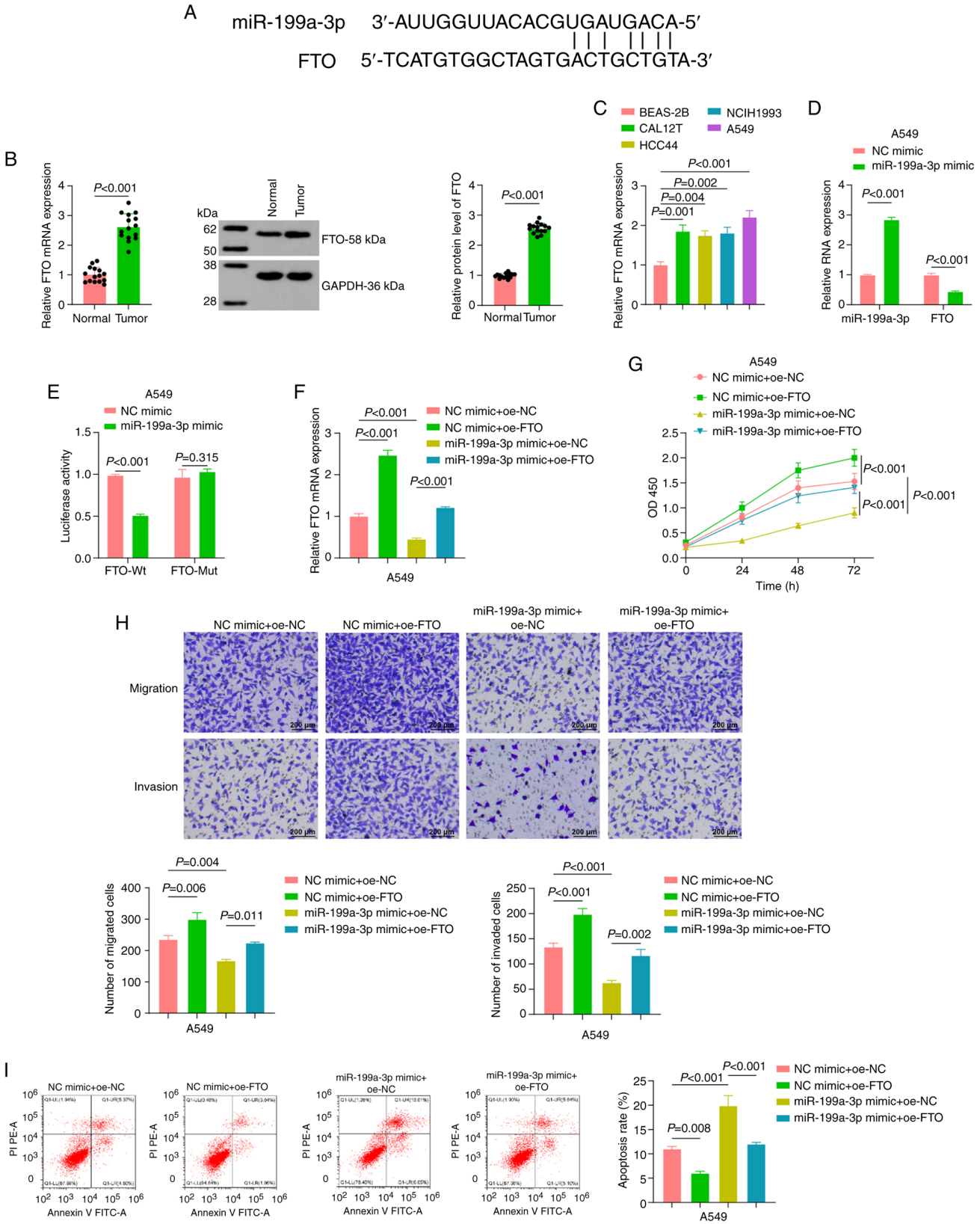

Figure 2. Effect of miR-199a-3p on the biological function of A549 cells by downregulating FTO. (A) Bioinformatics tool 'miRwalk' predicted the possible downstream target gene of miR-199a-3p: FTO. (B) RT-qPCR and western blot analysis were performed to detect the expression levels of FTO in non-small cell lung cancer tissues, with paracancerous tissues as the control (n=15). (C) RT-qPCR was performed to detect the expression levels of FTO in lung cancer cells. (D) After miR-199a-3p mimic transfection, RT-qPCR was used to detect the expression levels of miR-199a-3p and FTO. (E) A dual-luciferase reporter assay verified the targeting relationship between miR-199a-3p and FTO. (F) RT-qPCR was used to assess the expression levels of FTO in A549 cells in each miR mimic + oe plasmid combination group. (G) Cell Counting Kit-8 assay assessing the proliferation of A549 cells in each miR mimic + oe plasmid combination group. (H) Transwell assays indicated the migration and invasion of A549 cells in each miR mimic + oe plasmid combination group. Scale bar, 200 μm. (I) Flow cytometry was performed to detect the apoptosis of A549 cells in each miR mimic + oe plasmid combination group. Data are presented as the mean ± SEM, n=3 independent experiments. oe, overexpression; RT-qPCR, reverse transcription-quantitative PCR; miR, microRNA; FTO, fat mass and obesity-associated protein; NC, negative control; Wt, wild-type; Mut, mutant; OD, optical density.

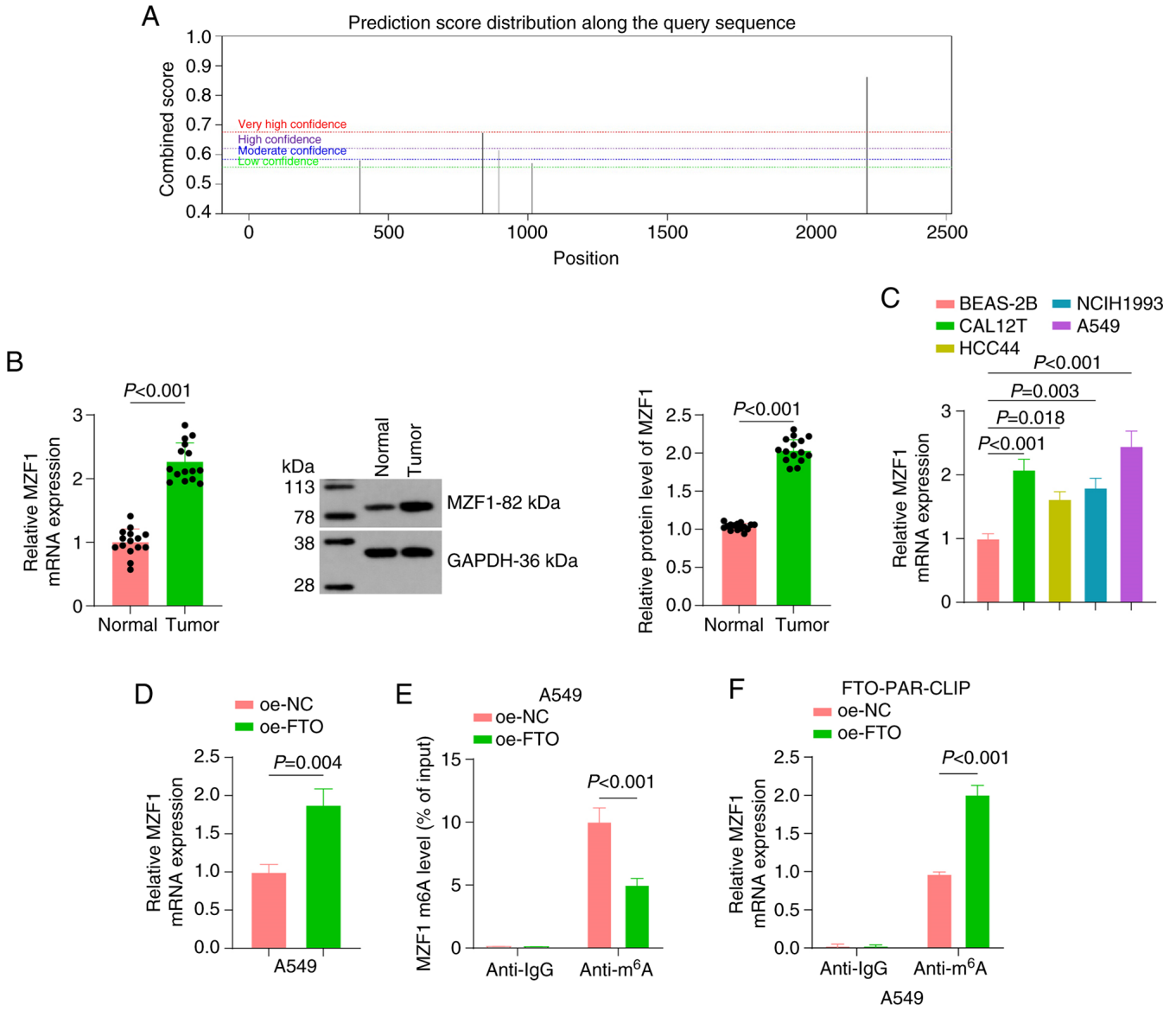

Figure 3. Mechanism of m^{6}A modification regulation of MZF1 by FTO. (A) The SRAMP online tool (http://www.cuilab.cn/sramp) predicted potential m^{6}A modification sites on MZF1 mRNA. (B) RT-qPCR and western blot analysis were conducted to assess the expression levels of MZF1 in NSCLC tissues, with paracancerous tissues as the control (n=15). (C) RT-qPCR analysis of MZF1 mRNA expression in normal bronchial epithelial (BEAS-2B) and NSCLC cell lines (CAL12T, HCC44, NCIH1993 and A549). (D) RT-qPCR was used to determine MZF1 expression after overexpression of FTO. (E) Methylated RNA immunoprecipitation assay detecting the m^{6}A modification level of MZF1 after overexpression of FTO. (F) PAR-CLIP assay detecting the direct interaction between FTO and MZF1 mRNA. All cell experiments were repeated three times. oe, overexpression; m^{6}A, N^6-methyladenosine; MZF1, myeloid zinc finger 1; FTO, fat mass and obesity-associated protein; RT-qPCR, reverse transcription-quantitative PCR; NSCLC, non-small cell lung cancer; NC, negative control; PAR-CLIP, photoactivatable ribonucleoside-enhanced crosslinking and immunoprecipitation.

and invasion of A549 cells were evaluated. RT-qPCR results revealed that the expression levels of both MZF1 and CLDND1 were significantly elevated in the cells of the oe-MZF1 + sh-NC group compared with those in the oe-NC + sh-NC group. Furthermore, the expression levels of CLDND1 were lower in the oe-MZF1 + sh-CLDND1 group than in the oe-MZF1 + sh-NC group (Fig. 6A). Functional experiments demonstrated that cell proliferation, migration and invasion were significantly increased, and apoptosis was significantly decreased in the oe-MZF1 + sh-NC group compared with the oe-NC + sh-NC group. When CLDND1 was silenced, the effect of MZF1 on A549 cell proliferation, migration, invasion and apoptosis was partially reversed (Fig. 6B-D).

In summary, these data indicated that MZF1 enhanced the proliferation, migration and invasion of A549 cells by promoting the transcription of CLDND1, and that the silencing of CLDND1 effectively inhibited these effects.

Discussion

Despite advances in research and treatment, lung cancer remains a notable threat to human health, with a low 5-year survival rate (37). Therefore, there is a need to develop reliable preclinical models and effective treatments. The findings of the present study contributed to the understanding of the molecular mechanisms underlying lung cancer and may provide novel targets for the development of molecularly targeted therapies (38).

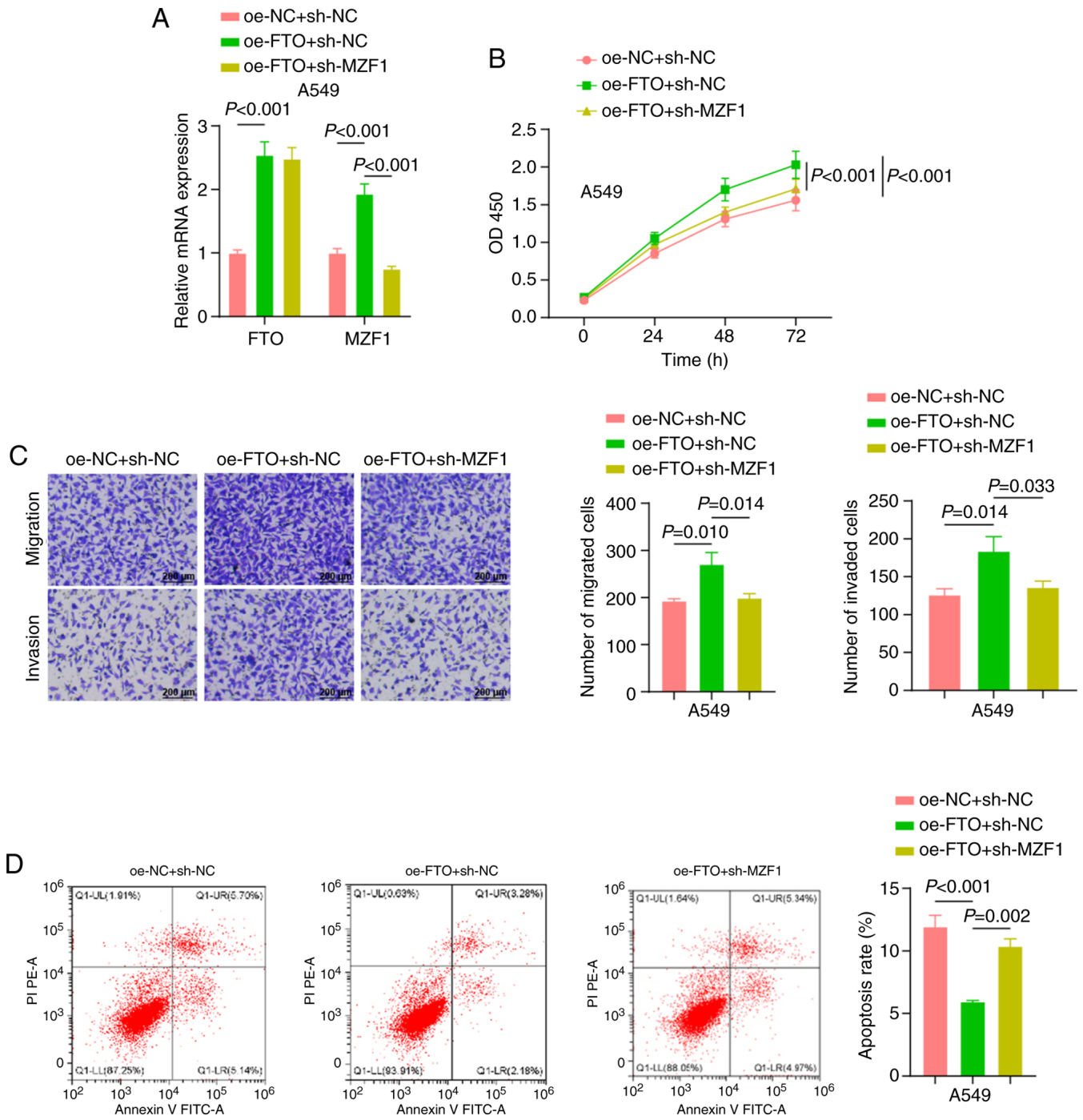

Figure 4. Effect of FTO on the biological function of A549 cells via regulation of MZF1. (A) Reverse transcription-quantitative PCR was performed to detect the expression levels of FTO and MZF1 in A549 cells in each oe plasmid + shRNA combination group. (B) Cell Counting Kit-8 assay examining the proliferation of A549 cells in each oe plasmid + shRNA combination group. (C) Transwell assay assessing the migration and invasion of A549 cells in each oe plasmid + shRNA combination group. Scale bar, 200 μm. (D) Flow cytometry was conducted to detect the apoptosis of A549 cells. All cell experiments were repeated three times. oe, overexpression; NC, negative control; sh, short hairpin RNA; FTO, fat mass and obesity-associated protein; MZF1, myeloid zinc finger 1; OD, optical density.

Aberrant miR-199a-3p expression has been observed in various cancer types and exhibits tumor suppressor effects. In one study, miR-199a-3p was shown to inhibit tumor growth *in vivo* and suppress the invasion and migration of nasopharyngeal carcinoma cells by downregulating the expression of stearoyl-CoA desaturase 1, thus providing a potential target for the treatment of nasopharyngeal carcinoma (9). Furthermore, miR-199a-3p is downregulated in various human malignancies, including hepatocellular carcinoma (HCC), leading to poor prognosis in patients with HCC (39). In HCC, knockdown of zinc finger and homeoboxes-1 (ZHX1) inhibits the upregulation of p53-upregulated modulator of apoptosis (PUMA) following miR-199a-3p transfection. Furthermore, silencing of either ZHX1 or PUMA reverses the effects of miR-199a-3p (40). One study has predicted that miR-199a-5p and miR-199a-3p can serve as early diagnostic markers or

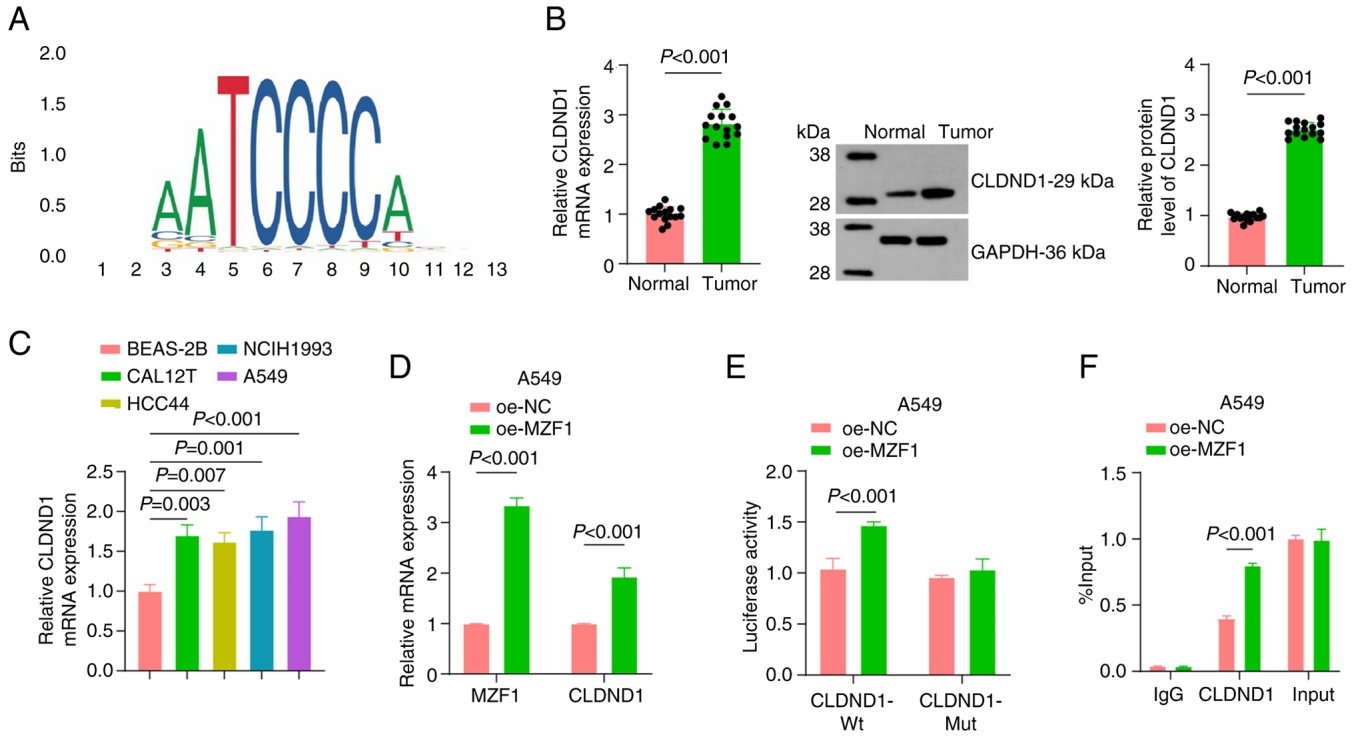

Figure 5. Mechanism of the transcriptional regulation of CLDND1 by MZF1. (A) The JASPAR website (https://jaspar.genereg.net/) was used to retrieve the binding site of the transcription factor MZF1. (B) RT-qPCR and western blot analysis were performed to detect the expression levels of CLDND1 in non-small cell lung cancer tissues, using paracancerous tissues as the control (n=15). (C) RT-qPCR analysis of CLDND1 mRNA expression in normal bronchial epithelial (BEAS-2B) and NSCLC cell lines (CAL12T, HCC44, NCIH1993 and A549). (D) After overexpression of MZF1, RT-qPCR was performed to measure MZF1 and CLDND1 expression. (E) Dual-luciferase reporter assay examining the effect of MZF1 on CLDND1 promoter activity. (F) Chromatin immunoprecipitation assays determining the enrichment of MZF1 in the CLDND1 promoter region [Chr3:167, 450, 703-167, 450, 714 (hg38)]. All cell experiments were repeated three times. oe, overexpression; CLDND1, claudin domain-containing 1; MZF1, myeloid zinc finger 1; RT-qPCR, reverse transcription-quantitative PCR; NC, negative control; Wt, wild-type; Mut, mutant.

therapeutic targets in NSCLC (6). However, the specific mechanism by which miR-199a-3p acts in lung cancer remains to be fully elucidated. Evidence supports the anticancer role of the miR-199a/Rheb/mTOR axis in NSCLC. Rheb, a common target of miR-199a-5p and miR-199a-3p, is involved in regulating the mTOR signaling pathway. Knockdown of Rheb recapitulated the tumor-suppressive effects of miR-199a overexpression, including inhibited proliferation and migration. Furthermore, miR-199a-5p/3p enhances the sensitivity of EGFR-T790M mutant NSCLC cells to (6). Taken together, these findings demonstrate that miR-199a-5p/3p can serve as an oncogene that inhibits the mTOR signaling pathway by targeting Rheb, thus inhibiting the regulatory process of NSCLC (6).

The present study explored a novel regulatory mechanism: miR-199a-3p targeted FTO to regulate the m^{6}A modification of MZF1, thus inhibiting CLDND1 expression, which provided a novel perspective to understand the function of miR-199a-3p in NSCLC. Observations revealed that miR-199a-3p was downregulated in NSCLC tissues and cells, and it had a direct targeting relationship with FTO. By targeting and inhibiting FTO, miR-199a-3p suppressed the migration, proliferation and invasion of A549 cells. FTO promoted MZF1 expression by decreasing the level of m^{6}A modification of MZF1. In addition, silencing of MZF1 reversed the promoting effect of FTO on lung cancer cell migration, proliferation and invasion. Furthermore, MZF1 promoted A549 cell migration, proliferation and invasion by promoting CLDND1 transcription.

Mechanistically, estrogen receptor α (ESR1) serves as the target for FTO, where heightened FTO expression decreases the m^{6}A levels in ESR1 mRNA (14). A study by Xu *et al* (14) reported two distinct m^{6}A modification sites, 5409A and 5247A, located in the 3'-UTR of ESR1, with FTO capable of reducing their methylation. In addition, the m^{6}A readers insulin-like growth factor 2 mRNA-binding protein (IGF2BP)3 and YTH domain-containing family protein 1 (YTHDF1) identify and bind to these m^{6}A sites, thereby enhancing ESR1 mRNA stability and promoting tumor growth. ESR1 was also found to exhibit diagnostic potential for NSCLC. In summary, the study by Xu *et al* (14) elucidated an important mechanism by which the FTO/YTHDF1/IGF2BP3/ESR1 axis regulates the epithelial transcriptome and highlighted the potential of m^{6}A-dependent NSCLC therapeutic strategies.

The data in the present study revealed that FTO stabilized MZF1 by removing its m^{6}A modification, thereby linking RNA methylation changes to the CLDND1-driven processes of cell migration and invasion. Notably, the study by Xu *et al* (14) proposed that FTO exerted an oncogenic effect by stabilizing ESR1, while another study has suggested that FTO has a tumor-suppressive effect in adenocarcinoma models (41). These discrepancies may stem from cell-type specificity, for example, adenocarcinoma vs. squamous cell carcinoma or different microenvironments, as well as variations in

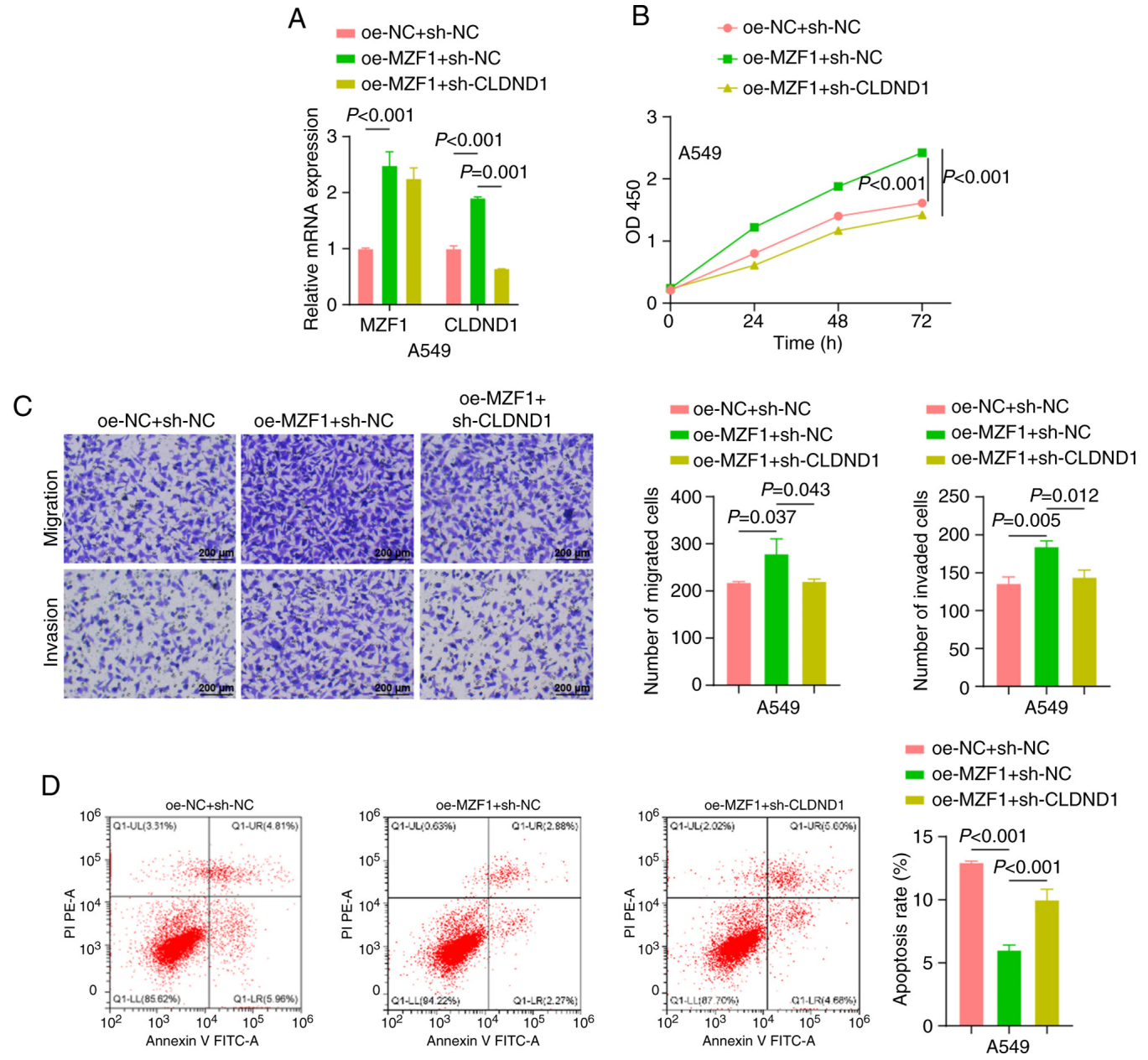

Figure 6. Effect of MZF1 on the biological function of lung cancer cells via regulation of CLDND1. (A) Reverse transcription-quantitative PCR was performed to detect the expression levels of MZF1 and CLDND1 in A549 cells in each group. (B) Cell Counting Kit-8 assay of the proliferation of A549 cells in each group. (C) Transwell assay examining the migration and invasion of A549 cells in each group. Scale bar, 200 μm. (D) Flow cytometry was performed to detect the apoptosis of A549 cells in each group. comparisons. All cell experiments were repeated three times. MZF1, myeloid zinc finger 1; CLDND1, claudin domain-containing 1; oe, overexpression; NC, negative control; sh, short hairpin RNA; OD, optical density.

downstream targets. The findings of the present study supported the oncogenic role of FTO through the stabilization of MZF1 and underscored the need for future validation of the translational potential of FTO in models based on EGFR mutation types or immune therapy resistance backgrounds. In summary, FTO may possess dual regulatory functions in lung cancer, with specific modes of action potentially depending on cancer subtype, target gene context and microenvironmental differences, which are factors that should be further clarified in future research.

Regulation of MZF1 signaling has been associated with the progression of numerous human malignancies, such as triple-negative breast and cervical cancer (42). Silencing of MZF1 inhibits cell proliferation, whereas its aberrant expression contributes to cancer development (43). Limited research exists on the specific mechanisms underlying the m^{6}A modification of MZF1 in lung cancer, which supports the novelty of the present study in exploring novel therapeutic regulatory mechanisms in this context. Furthermore, CLDND1, as a tight junction-associated protein, interacts with other tight junction proteins, such as occludin and claudins, to collectively construct and maintain the intact structure of intercellular tight junctions, forming a selective barrier that strictly regulates the transport of substances between cells and the conduction of intercellular signals, which is important for maintaining the stability of the tissue internal environment (18,44).

The role of CLDND1 during cancer progression has also attracted attention. Changes in CLDND1 expression are closely related to tumor development in certain cancer types, such as breast cancer (19). The inhibitory effect of gefitinib, an EGFR tyrosine kinase inhibitor, on CLDND1 expression has been evaluated using a luciferase reporter and ELK1 overexpression in ChIP assays. ELK1, identified as an enhancer region activator, transiently elevated CLDND1 expression at both the mRNA and protein levels. EGF-induced phosphorylation of ELK1 further increased CLDND1 expression, which was inhibited by gefitinib (19). Thus, EGF-dependent activation of ELK1 leads to the induction of CLDND1 expression. These findings pave the way for the development of novel anticancer drugs targeting CLDND1 (19). The present study revealed a significant increase in the enrichment of MZF1 in the promoter region of CLDND1 using ChIP experiments, supporting its direct action on the CLDND1 promoter. The present study also identified a novel role for CLDND1 in the malignant progression of tumors. A previous study has focused on the effects of CLDND1 on endothelial cell adhesion and cell junctions (45). However, the present study demonstrated that once transcriptionally activated by MZF1, CLDND1 also promoted malignant tumor phenotypes.

Based on the aforementioned analysis, miR-199a-3p was lowly expressed in NSCLC cells, which led to a weakening of its inhibitory effect on FTO, which in turn increased the expression levels of FTO. FTO, as an m^6A demethylase, removed m^6A modifications on the MZF1 mRNA, improved the mRNA stability and translational efficiency of MZF1 and increased the protein levels of MZF1. Subsequently, MZF1, as a transcription factor, upregulated the expression levels of CLDND1. The high expression of CLDND1 promoted malignant biological behaviors such as migration, proliferation and invasion of NSCLC cells. In summary, miR-199a-3p regulated the m^6A modification of MZF1 by targeting FTO, resulting in the inhibition of CLDND1 expression, which ultimately affected the biological functions of NSCLC cells.

Although the present study primarily focused on the axis of miR-199a-3p/FTO-mediated m^6A modification of MZF1 and its transcriptional regulation of CLDND1, the present study did not systematically exclude the involvement of other key factors. The stability and translational efficiency of MZF1 may have also been regulated by m^6A reader proteins, including the IGF2BP family and YTHDF1/2/3 (46). m^6A methyltransferases and demethylases such as methyltransferase-like protein 3/14 and alkylated DNA repair protein alkB homolog 5 may have also indirectly intervened by regulating the expression of MZF1 (47); and iii) in addition to MZF1, there may have been other cis-acting elements and binding proteins on the CLDND1 promoter (19,48). As the present study did not conduct m^6A site prediction, enrichment analysis or RNA immunoprecipitation validation of the reader proteins, the relevant regulatory mechanisms require further exploration.

The present study also had certain limitations. The small sample size in the present study may undermine the universality of the molecular associations among miR-199a-3p, FTO, MZF1, and CLDND1, potentially limiting the reliability of clinical relevance analysis. Furthermore, the present study relied on *in vitro* cell experiments and lacked data from *in vivo* animal models, making it difficult to comprehensively evaluate the role of this pathway in living tumors. Additionally, the signaling pathways in NSCLC cells are complex, and the factors in the present study may have participated in multiple pathways, necessitating further research with expanded samples to explore their interrelationships and mechanisms.

In conclusion, miR-199a-3p targeted and inhibited FTO expression, thereby blocking the m^6A demethylation modification of MZF1 and suppressing MZF1 expression and the transcriptional activation of downstream CLDND1 (Fig. S2). This ultimately inhibited the migration, proliferation and invasion of NSCLC cells. The aforementioned mechanism suggested that the miR-199a-3p/FTO/MZF1/CLDN1 signaling pathway serves an important role in the development and progression of NSCLC. Unlike the findings of a study by Xu *et al* (14) indicating that FTO participates in NSCLC progression by regulating ESR1, the present study is, to the best of our knowledge, the first to propose that miR-199a-3p targets and inhibits FTO, relieving its m^6A demethylation effect on MZF1 and indirectly inhibiting the MZF1-mediated transcriptional activation of CLDND1. To the best of our knowledge, this multi-level regulatory axis of miRNA-epigenetic modification/transcription factor/target gene has not been reported before. The present study explored a novel upstream regulator, miR-199a-3p, and downstream oncogenic mechanism, the MZF1/CLDND1 axis, of FTO in NSCLC, providing novel insights for m^6A-targeted therapy.

Future studies could validate the clinical significance of this signaling pathway in larger sample cohorts, study the association between the expression levels of miR-199a-3p, FTO, MZF1 and CLDND1, and clinical parameters such as TNM staging to enhance its clinical applicability, establish lung cancer xenograft models to simulate the human tumor microenvironment and validate the biological functions and therapeutic potential of this pathway, and test this signaling axis in models with EGFR mutations or immune therapy resistance to explore its roles in different lung cancer subtypes and treatment resistance scenarios, providing novel targets and strategies for precision therapy. m^6A reader protein in RNA pull-down experiments will be supplemented in the future to further refine the analysis of the regulatory pathway network.

Acknowledgements

Not applicable.

Funding

The present study was supported by the Application Foundation Project of Yanbian University in 2024 (grant no. ydkj202458).

Availability of data and materials

The data generated in the present study may be requested from the corresponding author.

Authors' contributions

YC conceived and designed the study. XL performed the experiments. HZ, WY and EZ conducted the data analysis and

interpretation. WY and EZ edited the manuscript. YC and HZ confirm the authenticity of all the raw data. All authors read and approved the final version of the manuscript.

Ethics approval and consent to participate

The present study was approved by the Ethics Committee of Yanbian University Affiliated Hospital (approval no. 2021094; Yanji, China) and written informed consent was obtained from the patients. The study followed The Declaration of Helsinki.

Patient consent for publication

Not applicable.

Competing interests

The authors declare that they have no competing interests.

References

1. Yang H, Liu Y, Chen L, Zhao J, Guo M, Zhao X, Wen Z, He Z, Chen C and Xu L: MiRNA-based therapies for lung cancer: Opportunities and challenges? Biomolecules 13: 877, 2023.
2. Ruiz-Cordero R and Devine WP: Targeted therapy and checkpoint immunotherapy in lung cancer. Surg Pathol Clin 13: 17-33, 2020.
3. Wang K, Mei Z, Zheng M, Liu X, Li D and Wang H: FTO-mediated autophagy inhibition promotes non-small cell lung cancer progression by reducing the stability of SESN2 mRNA. Heliyon 10: e27571, 2024.
4. Zahmatyar M, Kharaz L, Abiri Jahromi N, Jahanian A, Shokri P and Nejadghaderi SA: The safety and efficacy of binimetinib for lung cancer: A systematic review. BMC Pulm Med 24: 379, 2024.
5. van Zandwijk N, Pavlakis N, Kao SC, Linton A, Boyer MJ, Clarke S, Huynh Y, Chrzanowska A, Fulham MJ, Bailey DL, *et al*: Safety and activity of microRNA-loaded minicells in patients with recurrent malignant pleural mesothelioma: a first-in-man, phase 1, open-label, dose-escalation study. Lancet Oncol 18: 1386-1396, 2017.
6. Liu X, Wang X, Chai B, Wu Z, Gu Z, Zou H, Zhang H, Li Y, Sun Q, Fang W and Ma Z: miR-199a-3p/5p regulate tumorgenesis via targeting Rheb in non-small cell lung cancer. Int J Biol Sci 18: 4187-4202, 2022.
7. Meng W, Li Y, Chai B, Liu X and Ma Z: miR-199a: A tumor suppressor with noncoding RNA network and therapeutic candidate in lung cancer. Int J Mol Sci 23: 8518, 2022.
8. Hou G, Wang Y, Zhang M, Hu Y, Zhao Y, Jia A, Wang P, Zhao W, Zhao W and Lu Z: miR-199a-3p suppresses progression of esophageal squamous cell carcinoma through inhibiting mTOR/p70S6K pathway. Anticancer Drugs 32: 157-167, 2021.
9. Hu W, Wang Y, Zhang Q, Luo Q, Huang N, Chen R, Tang X, Li X and Luo H: MicroRNA-199a-3p suppresses the invasion and metastasis of nasopharyngeal carcinoma through SCD1/PTEN/AKT signaling pathway. Cell Signal 110: 110833, 2023.
10. Wei H, Li Z, Liu F, Wang Y, Ding S, Chen Y and Liu J: The role of FTO in tumors and its research progress. Curr Med Chem 29: 924-933, 2022.
11. Azzam SK, Alsafar H and Sajini AA: FTO m6A demethylase in obesity and cancer: Implications and underlying molecular mechanisms. Int J Mol Sci 23: 3800, 2022.
12. Zaccara S, Ries RJ and Jaffrey SR: Publisher correction: Reading, writing and erasing mRNA methylation. Nat Rev Mol Cell Biol 24: 770, 2023.
13. Yang Z, Yu GL, Zhu X, Peng TH and Lv YC: Critical roles of FTO-mediated mRNA m6A demethylation in regulating adipogenesis and lipid metabolism: Implications in lipid metabolic disorders. Genes Dis 9: 51-61, 2021.
14. Xu X, Qiu S, Zeng B, Huang Y, Wang X, Li F, Yang Y, Cao L, Zhang X, Wang J and Ma L: N^6-methyladenosine demethyltransferase FTO mediated m^6A modification of estrogen receptor alpha in non-small cell lung cancer tumorigenesis. Oncogene 43: 1288-1302, 2024.
15. Zhang ZW, Zhao XS, Guo H and Huang XJ: The role of m^6A demethylase FTO in chemotherapy resistance mediating acute myeloid leukemia relapse. Cell Death Discov 9: 225, 2023.
16. Wu D, Tan H, Su W, Cheng D, Wang G, Wang J, Ma DA, Dong GM and Sun P: MZF1 mediates oncogene-induced senescence by promoting the transcription of p16(INK4A). Oncogene 41: 414-426, 2022.
17. Wang CH, Wu HC, Hsu CW, Chang YW, Ko CY, Hsu TI, Chuang JY, Tseng TH and Wang SM: Inhibition of MZF1/c-MYC Axis by cantharidin impairs cell proliferation in glioblastoma. Int J Mol Sci 23: 14727, 2022.
18. Ohnishi M, Ochiai H, Matsuoka K, Akagi M, Nakayama Y, Shima A, Uda A, Matsuoka H, Kamishikiryo J, Michihara A and Inoue A: Claudin domain containing 1 contributing to endothelial cell adhesion decreases in presence of cerebellar hemorrhage. J Neurosci Res 95: 2051-2058, 2017.
19. Matsuoka H, Yamaoka A, Hamashima T, Shima A, Kosako M, Tahara Y, Kamishikiryo J and Michihara A: EGF-dependent activation of ELK1 contributes to the induction of CLDND1 expression involved in tight junction formation. Biomedicines 10: 1792, 2022.
20. Yin H, Chen L, Piao S, Wang Y, Li Z, Lin Y, Tang X, Zhang H, Zhang H and Wang X: M6A RNA methylation-mediated RMRP stability renders proliferation and progression of non-small cell lung cancer through regulating TGFBR1/SMAD2/SMAD3 pathway. Cell Death Differ 30: 605-617, 2023.
21. Livak KJ and Schmittgen TD: Analysis of relative gene expression data using real-time quantitative PCR and the 2(-Delta Delta C(T)) method. Methods 25: 402-408, 2001.
22. Gong Y, Li X and Xie L: Circ_0001897 regulates high glucose-induced angiogenesis and inflammation in retinal microvascular endothelial cells through miR-29c-3p/transforming growth factor beta 2 axis. Bioengineered 13: 11694-11705, 2022.
23. Robinson R, Srinivasan M, Shanmugam A, Ward A, Ganapathy V, Bloom J, Sharma A and Sharma S: Interleukin-6 trans-signaling inhibition prevents oxidative stress in a mouse model of early diabetic retinopathy. Redox Biol 34: 101574, 2020.
24. Liu P, Peng QH, Tong P and Li WJ: Astragalus polysaccharides suppresses high glucose-induced metabolic memory in retinal pigment epithelial cells through inhibiting mitochondrial dysfunction-induced apoptosis by regulating miR-195. Mol Med 25: 21, 2019.
25. Zhao G, Liang J, Shan G, Gu J, Xu F, Lu C, Ma T, Bi G, Zhan C and Ge D: KLF11 regulates lung adenocarcinoma ferroptosis and chemosensitivity by suppressing GPX4. Commun Biol 6: 570, 2023.
26. Zhang W, Ruan X, Li Y, Zhi J, Hu L, Hou X, Shi X, Wang X, Wang J, Ma W, *et al*: KDM1A promotes thyroid cancer progression and maintains stemness through the Wnt/β-catenin signaling pathway. Theranostics 12: 1500-1517, 2022.
27. Dominissini D, Moshitch-Moshkovitz S, Schwartz S, Salmon-Divon M, Ungar L, Osenberg S, Cesarkas K, Jacob-Hirsch J, Amariglio N, Kupiec M, *et al*: Topology of the human and mouse m6A RNA methylomes revealed by m6A-seq. Nature 485: 201-206, 2012.
28. Lin S, Xu H, Qin L, Pang M, Wang Z, Gu M, Zhang L, Zhao C, Hao X, Zhang Z, *et al*: UHRF1/DNMT1-MZF1 axis-modulated intragenic site-specific CpGI methylation confers divergent expression and opposing functions of PRSS3 isoforms in lung cancer. Acta Pharm Sin B 13: 2086-2106, 2023.
29. Wang F, Hou W, Li X, Lu L, Huang T, Zhu M and Miao C: SETD8 cooperates with MZF1 to participate in hyperglycemia-induced endothelial inflammation via elevation of WNT5A levels in diabetic nephropathy. Cell Mol Biol Lett 27: 30, 2022.
30. Xue X, Wang M, Zhang X, Ma L and Wang J: PAR-CLIP assay in ferroptosis. Methods Mol Biol 2712: 29-43, 2023.
31. Hou Y, Zhang Q, Pang W, Hou L, Liang Y, Han X, Luo X, Wang P, Zhang X, Li L and Meng X: YTHDC1-mediated augmentation of miR-30d in repressing pancreatic tumorigenesis via attenuation of RUNX1-induced transcriptional activation of Warburg effect. Cell Death Differ 28: 3105-3124, 2021.
32. Liu L, Xie D, Xie H, Huang W, Zhang J, Jin W, Jiang W and Xie D: ARHGAP10 inhibits the proliferation and metastasis of CRC cells via blocking the activity of RhoA/AKT signaling pathway. Onco Targets Ther 12: 11507-11516, 2019.
33. Zhang G, Wang L, Zhao L, Yang F, Lu C, Yan J, Zhang S, Wang H and Li Y: Silibinin induces both apoptosis and necroptosis with potential anti-tumor efficacy in lung cancer. Anticancer Agents Med Chem 24: 1327-1338, 2024.

34. Iqbal MA, Arora S, Prakasam G, Calin GA and Syed MA: MicroRNA in lung cancer: Role, mechanisms, pathways and therapeutic relevance. Mol Aspects Med 70: 3-20, 2019.
35. Kan A, Liu S, He M, Wen D, Deng H, Huang L, Lai Z, Huang Y and Shi M: MZF1 promotes tumour progression and resistance to anti-PD-L1 antibody treatment in hepatocellular carcinoma. JHEP Rep 6: 100939, 2023.
36. Brix DM, Bundgaard Clemmensen KK and Kallunki T: Zinc finger transcription factor MZF1-A specific regulator of cancer invasion. Cells 9: 223, 2020.
37. Meng FT, Jhuang JR, Peng YT, Chiang CJ, Yang YW, Huang CY, Huang KP and Lee WC: Predicting lung cancer survival to the future: Population-based cancer survival modeling study. JMIR Public Health Surveill 10: e46737, 2024.
38. Li H, Chen Z, Chen N, Fan Y, Xu Y and Xu X: Applications of lung cancer organoids in precision medicine: From bench to bedside. Cell Commun Signal 21: 350, 2023.
39. Chen G, Zhang Z, Li Y, Wang L and Liu Y: LncRNA PTPRG-AS1 promotes the metastasis of hepatocellular carcinoma by enhancing YWHAG. J Oncol 2021: 3624306, 2021.
40. Guan J, Liu Z, Xiao M, Hao F, Wang C, Chen Y, Lu Y and Liang J: MicroRNA-199a-3p inhibits tumorigenesis of hepatocellular carcinoma cells by targeting ZHX1/PUMA signal. Am J Transl Res 9: 2457-2465, 2017.
41. Wu G, Yan Y, Cai Y, Peng B, Li J, Huang J, Xu Z and Zhou J: ALKBH1-8 and FTO: Potential therapeutic targets and prognostic biomarkers in lung adenocarcinoma pathogenesis. Front Cell Dev Biol 9: 633927, 2021.
42. Yue CH, Liu JY, Chi CS, Hu CW, Tan KT, Huang FM, Pan YR, Lin KI and Lee CJ: Myeloid zinc finger 1 (MZF1) maintains the mesenchymal phenotype by down-regulating IGF1R/p38 MAPK/ERα signaling pathway in high-level MZF1-expressing TNBC cells. Anticancer Res 39: 4149-4164, 2019.
43. Mudduluru G, Vajkoczy P and Allgayer H: Myeloid zinc finger 1 induces migration, invasion, and in vivo metastasis through Axl gene expression in solid cancer. Mol Cancer Res 8: 159-169, 2010.
44. Matsuoka H, Shima A, Uda A, Ezaki H and Michihara A: The retinoic acid receptor-related orphan receptor α positively regulates tight junction protein claudin domain-containing 1 mRNA expression in human brain endothelial cells. J Biochem 161: 441-450, 2017.
45. Shima A, Matsuoka H, Yamaoka A and Michihara A: Transcription of CLDND1 in human brain endothelial cells is regulated by the myeloid zinc finger 1. Clin Exp Pharmacol Physiol 48: 260-269, 2021.
46. Huang H, Weng H, Sun W, Qin X, Shi H, Wu H, Zhao BS, Mesquita A, Liu C, Yuan CL, *et al*: Recognition of RNA N^6-methyladenosine by IGF2BP proteins enhances mRNA stability and translation. Nat Cell Biol 20: 285-295, 2018.
47. Liu J, Ren D, Du Z, Wang H, Zhang H and Jin Y: m^6A demethylase FTO facilitates tumor progression in lung squamous cell carcinoma by regulating MZF1 expression. Biochem Biophys Res Commun 502: 456-464, 2018.
48. Sun J, Liu P and Wang X: MiR-595 and Cldnd1: Potential related factors for bone loss in postmenopausal women with hip osteoporotic fracture. PLoS One 19: e0313106, 2024.